THE BELL SYSTEM TECHNICAL JOURNAL
Vol. 59, No. 1, January 1980
Printed in U.S.A.

Copper Conductivity at Millimeter-Wave Frequencies

By L. W. HINDERKS and A. MAIONE

(Manuscript received June 8, 1979)

Copper was electrodeposited on steel substrates and annealed at 300°C in a nitrogen-filled oven. The conductivities of the deposits, measured at 43 GHz, were between 82 and 93 percent of the IACS (International Annealed Copper Standard) value of 5.8 × 10^7 S/m. The conductivity of the plating is sensitive to minute changes in the concentration of copper cyanide and sodium cyanide in the plating solution. In all cases, the annealing step at 300°C effected a significant improvement in the copper conductivity. Special instrumentation was developed to permit accurate determination of the copper conductivity at millimeter-wave frequencies. An intrinsic accuracy of approximately 1 percent was achieved for the electrical measurement. When the variations due to the mechanical fixturing were included, the measured standard deviation for copper conductivities between 4.3 and 5.4 was typically 0.047 (×10^7 S/m).

I. INTRODUCTION

The conductivity of copper at 40 and 110 GHz has recently been reported as part of the Bell Laboratories WT-4 waveguide field evaluation trial (FET).[1] In this experiment, 14 kilometers of 60-mm waveguide was installed and measured. The interior of the steel waveguide was copper-plated and then lined with a thin polyethylene liner. The dielectric liner was used to modify the mode patterns in the waveguide.[2] The results of the FET indicated a copper conductivity at 42 GHz that was much higher than that usually experienced at millimeter-wave frequencies. This high conductivity was achieved for waveguide fabricated in a manufacturing environment.

A laboratory experiment was devised to isolate the process steps and the mechanism responsible for the high conductivity copper achieved. The results of this experiment are reported here.

Table I—Results summary

Experimenter	Frequency (GHz)	Percent IACS	Remarks
Thorpe	38	57	High purity copper
		78	Etched in acid
		98	Etched and annealed
Tischer	35	78	Single crystal high purity annealed and etched
Hatano and Nihei	40	62	51-mm waveguide TE_{01}, TE_{02}, TE_{03}, TE_{04}
Anderson et al	42	89	60-mm waveguide TE_{01}; Bell Labs FET
Hinderks and Maione	43	93	Plated and annealed

Various investigators have previously reported work on the conductivity of copper at millimeter-wave frequencies. J. S. Thorpe has reported conductivities at 38 GHz approaching the theoretical value as inferred from the IACS* value.[3,4] To achieve these conductivity results, it was found necessary to acid-etch and then anneal the copper samples in a hydrogen environment at 780°C. F. J. Tischer has reported work on high purity crystal samples of copper at 35 GHz.[5,6] Samples prepared for his experiments were carefully grown single crystals whose surfaces were etched to remove any possible surface contamination. Samples were transported and measured in an argon atmosphere to prevent surface oxidation. These samples, when measured, revealed a conductivity 78 percent IACS. Hatano and Nihei have measured the surface conductivity of copper waveguide, which was coated with a layer of copper oxide, by transmitting single pulse TE_{01}, TE_{02}, TE_{03}, and TE_{04} modes through 100-m lengths of 51-mm diameter waveguide.[7] These single pulse attenuation measurements all yielded values of conductivity which are 62 percent IACS.

The results of previous work and the work reported in this paper are summarized in Table I.

The Bell Laboratories studies are shown in the table. One was obtained from the 14-km FET and the second from a special Q set reported in this paper.

The test set designed to measure the copper conductivity was based on measuring the Q of a cavity. The cavity geometry (cylindrical) supported TE_{0N} modes and caused no discontinuities in current flow patterns. The design also confined all the significant losses to the surface being measured, while allowing for the consistent assembly and disassembly needed for looking at multistep processes. A microwave source having a narrow spectral output was used to excite the high Q cavity, and techniques were adopted to calibrate source frequency and output power. Also, all the data points (256) were used to estimate the resonance parameters. Finally, a number of data cross-

* International Annealed Copper Standard.

checking methods were employed to insure the integrity of the data. Particular care was taken to design fixtures that assured reproducible results. A microprocessor and a minicomputer were incorporated in the test set to automate data acquisition and to process the data to achieve the desired accuracy.

Since the specific execution of the test set and the data processing are of importance in addressing the measurement accuracy demonstrated, they are covered in some detail in the following paragraphs.

1.1 Q-set measurement theory (see Appendix A for detailed derivations)

The basic measurement consists of first computing the loaded Q of a circular TE_{01} cavity in the usual manner:

$$Q_L = \frac{f_o}{\Delta f}. \tag{1}$$

Next, the transmission loss T through the cavity is measured,

$$T = \frac{P_L}{P_o} \text{ (eq. (19), App. A)}, \tag{2}$$

where

P_L = power transmitted on resonance

P_o = power transmitted with cavity out of circuit. From Q_L and T, the unloaded Q, Q_o is computed:

$$Q_o = Q_L \left(\frac{1}{1 - \sqrt{T}}\right) \text{ (eq. (21), App. A)}. \tag{3}$$

The skin depth (δ) of the copper on the ends of the cavity can be determined as follows:

$$\delta_{\text{ends}} = \frac{[P_{01}^2 + (l\pi R/L)^2]^{3/2}}{(2R/L)(l\pi R/L)^2}\left[\frac{\lambda_o}{2\pi Q_o}\right] \text{ (eq. (10), App. A)}, \tag{4}$$

where

P_{01} = First root of the derivative of the zero-order Bessel function

R = radius of cavity

L = length of cavity

$\lambda_o = c/f$, c = speed of light, f = frequency

l = length of cavity in half wavelengths.

The effect of the side-wall term in computing the skin depth has been neglected.

The skin depth yields the conductivity (σ) directly from the well-known formula[8]

$$\sigma = \frac{1}{\pi f \mu_o \delta_{\text{ends}}^2},$$

where

f = frequency

μ_o = permeability of vacuum ($4\pi \times 10^{-7}$ Henries/meter).

II. TEST SET IMPLEMENTATION

2.1 *Electrical measurements and data acquisition*

The test set (Fig. 1) is implemented by a standard resonant transmission cavity technique. In this system, however, the requirement for high accuracy and repeatability is paramount. In the tests that are made, absolute accuracy on the order of a few percent is required. Typical cavity resonance widths must be measured to within 70 kHz because cavity Qs ($\approx$6000) imply resonance widths of 7 MHz. This frequency accuracy is difficult to achieve at 43 GHz. The high Qs of the cavities used require a microwave source that has a narrow spectral

Fig. 1—Copper conductivity test set.

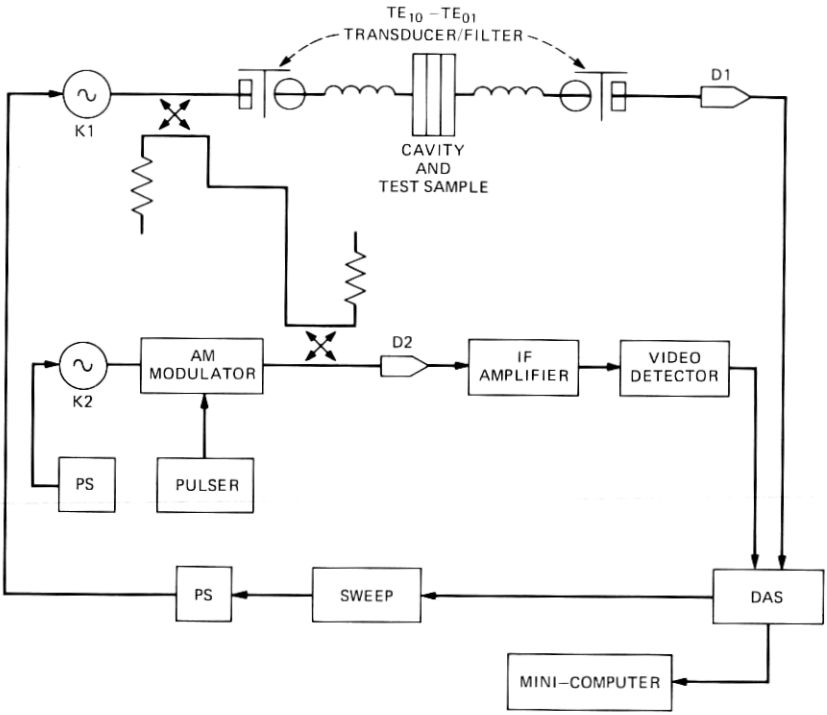

Fig. 2—Simplified diagram of Q set

output. Klystrons were chosen because of their spectral purity ($\Delta f \approx$ 100 kHz). Backward-wave oscillators have broad spectral characteristics ($\Delta f \approx$ 1 MHz) that are unsuitable for the accuracy required for these experiments. To prevent frequency drift, the klystrons were immersed in oil baths. Figure 2 is a simplified diagram of the test set. It is essentially a standard transmission cavity test set with the addition of a frequency marker system. In operation, the frequency source (K1) is swept through approximately 60 MHz while the transmitted power is monitored at detector D1. The marker system generates a picket fence spectrum with a frequency spacing of approximately 2 MHz between peaks. The marker system output is detected by detector D2.

A dual microprocessor data acquisition system (DAS), Fig. 3, serves as the test set controller. One microprocessor is dedicated to the data acquisition and the data link protocol, while the other microprocessor monitors the front panel keyboard and updates all readout devices. The data acquisition system allows up to three simultaneous real-time analog inputs to be displayed on the CRT readout.

Because the klystron source sweeps nonlinearly in frequency, a

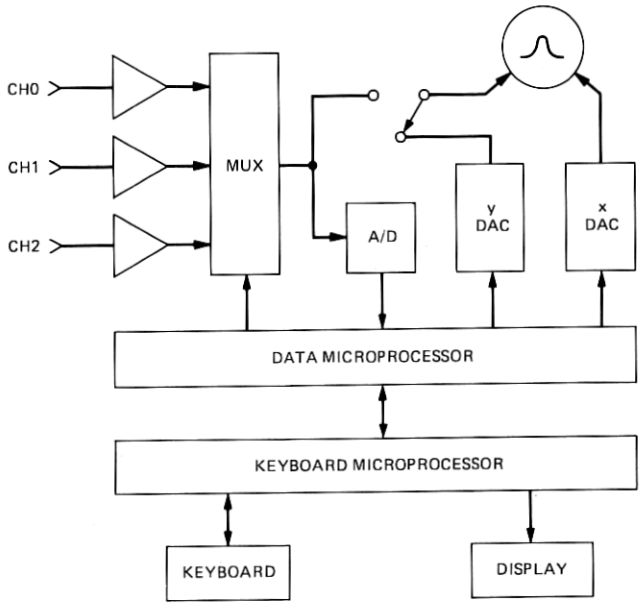

Fig. 3—Dual microprocessor data acquisition system.

mechanism to calibrate the sweep is required. This is the function of the marker system. This marker system consists of a picket fence constructed by AM-modulating a fixed frequency klystron K2 with a 10-ns pulse which has a repetition rate of approximately 2 MHz. Modulating K2 in this manner generates a comb spectrum approximately 200 MHz wide, with the teeth spaced every 2 MHz.

Klystron K1 is swept through the resonant frequency of the cavity while a portion of K1 is mixed with the comb spectrum. The transmission through the cavity is detected by detector D1 and digitized by the data acquisition system. The IF output of the marker system is amplified by an IF amplifier, video-detected by the video detector, and also digitized by the data acquisition system. Thus the data acquisition system simultaneously digitizes the transmission and marker data. The IF amplifier has a bandwidth of 0.5 MHz and a center frequency of 30 MHz.

Klystron K1 is swept by the sweeper circuit. This sweep generator produces a sawtooth waveform, which is used to sweep the klystron K1. The start of a sweep cycle is controlled by the data acquisition system. In this manner, the data acquisition system initiates a sweep and then subsequently digitizes 256 points for each of the two input channels to a resolution of 12 bits. The sweeper takes approximately 55 ms for one sweep.

The ability of the test set to average multiple sweeps allowed high signal-to-noise ratios to be achieved. Typical measurements involved averaging 102 sweeps to achieve a tenfold increase in signal to noise. The resulting s/n typically observed is 100.

The data acquisition system has the capability to observe the input signals in real time. The digitized data stored in memory can also be displayed. Both displays are presented on a small CRT screen which is part of the data acquisition system. The data acquisition system has programmable operational amplifiers whose gain can be set by the front panel keyboard. A programmable offset voltage can be added to the input signals before amplification. This allows capture of inputs that contain small dc biases.

III. CAVITY CONSTRUCTION

The choice of the millimeter-wave cavity configuration (cylindrical) was dictated by the requirement that the cavity should be assembled and disassembled easily without affecting the measurement repeatability. To achieve this goal, the TE_{01} and TE_{02} circular electrical modes were chosen as the test modes, since the cavity wall currents associated

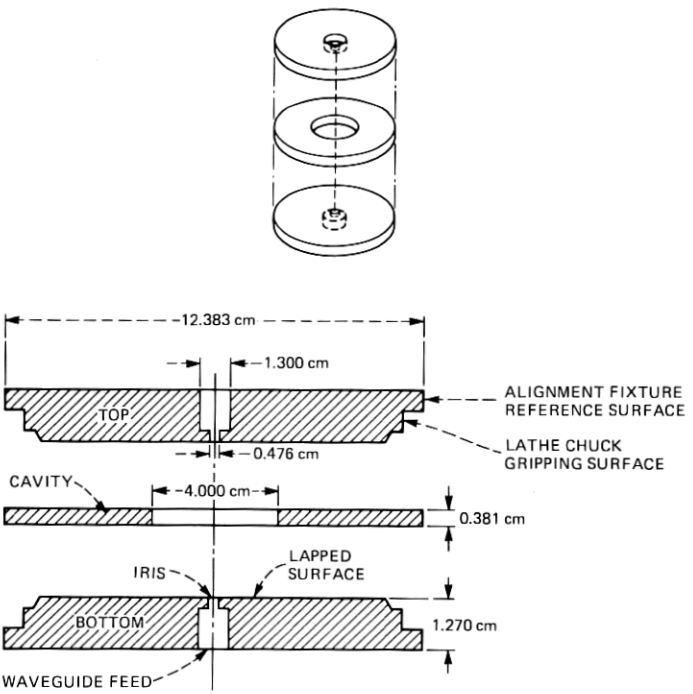

Fig. 4—Cavity design.

with them are circumferential. The cavity was constructed so that no electrical currents flowed across the joints of the cavity. In this manner, problems associated with cavity joint conductivity are essentially eliminated. Because the modes that were chosen are not the dominant mode of the cavity, extreme care in cavity construction was exercised to prevent the generation of spurious modes. Figure 4 depicts the cavity design and Fig. 5 shows one of the actual cavities used.

The fixturing necessary to guarantee the precise alignment needed for this cavity is shown in Fig. 6. The cavity alignment fixture utilizes a three-point alignment technique to align the three disks comprising the cavity assembly. Basically, it consists of two fixed points, provided by a stationary precision *V*-block mounted on a precision ground tool base, and one moving point, a precision *L*-block mounted on a unislide assembly with a crank. A provision for top (vertical) loading was also provided. This type of fixture design permits semiautomatic alignment with maximum consistency.

The complete cavity assembly is comprised of three precision steel disks: two identical disks each having an iris hole through its center forming the ends of the cavity and one washer-shaped disk that defines the geometry of the cavity (thickness and diameter). The cavity ends (top and bottom) are the actual copper-plated substrates under test. The iris hole, located at the disk center, is the mechanism for coupling the cavity to external circuits.

To prevent the generation of spurious modes in the cavity, precise mechanical tolerances were used, as opposed to mode suppression techniques. Loss from the desired mode caused by mode suppressors

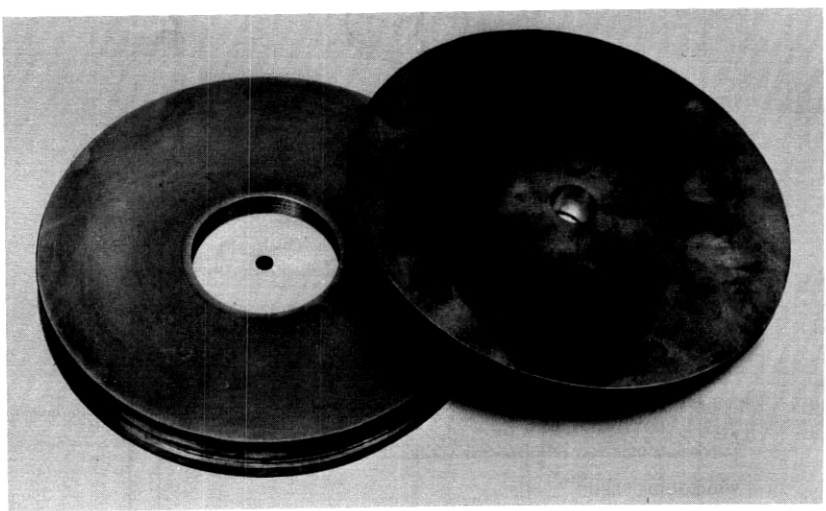

Fig. 5—TE_{01} cavity.

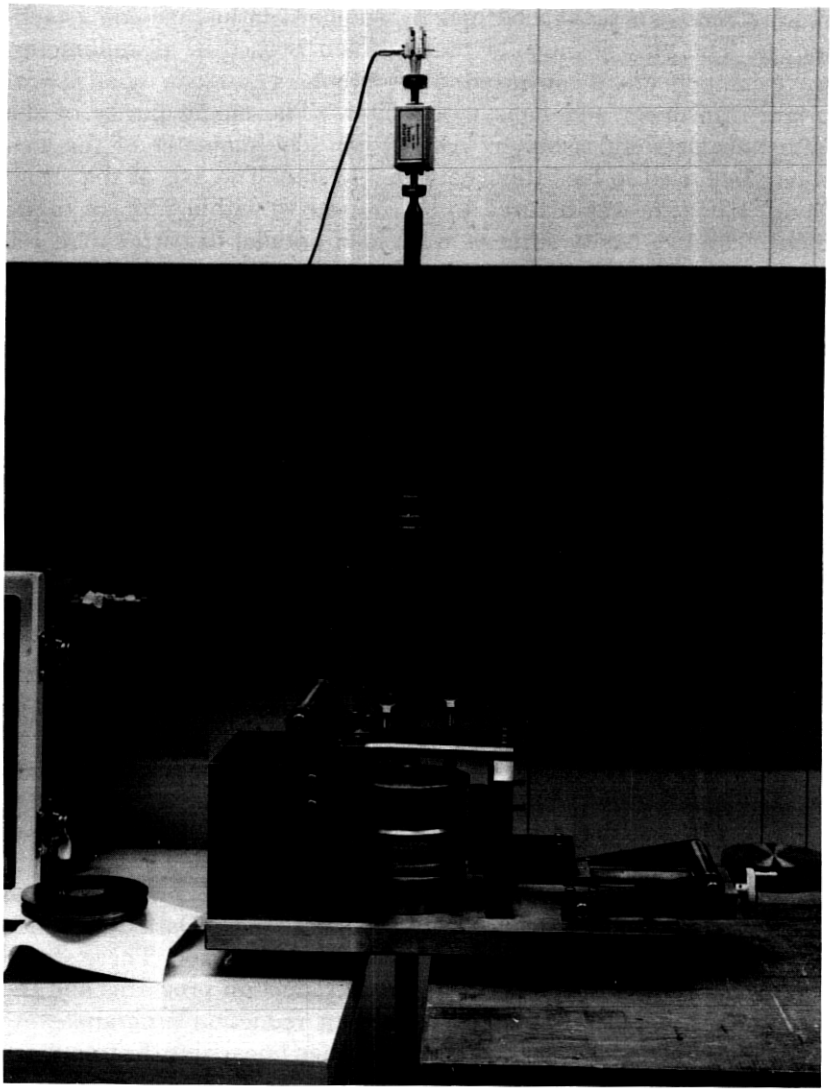

Fig. 6—Cavity/test fixture.

is extremely difficult to calculate, and thus the mode suppression technique was not used to prevent unwanted model generation. Precise mechanical tolerances were relatively easy to achieve because of the cavity geometry design. The substrates used to form the end walls of the cavity were typically machined and lapped to be flat over the region of interest to less than 0.25 μm (10 microinches). In addition, the surface roughness of these sample substrates was better than 0.25 μm. To insure the generation of only TE_{01} or TE_{02}, it is important

that the cavity be circularly symmetric about the iris axis. This requirement can readily be met by standard lathe-machining techniques. The TE_{10} rectangular mode, which is used in all millimeter-wave components, is converted to the circular TE_{01} mode by an appropriate transducer and helix mode filter.[9] The modal purity of the launching network is better than 40 dB. The diameter of the TE_{01} waveguide used to feed the cavity was 13 mm. The axis of the entire cavity structure was fixtured to be colinear to within 2.54 μm (0.001 inch). The two cavity surfaces were held parallel to better than 100 microradians by the cavity spacer. The system was assembled in the fixture shown in Fig. 6, and sufficient torque was applied to the cavity fixture to guarantee good molecular adhesion between all critical mating surfaces.

IV. DATA TRANSPORT

The raw data acquired by the DAS are transported to a host minicomputer for processing (see Appendix C). To assure reliable communication between the DAS and the host, a special-purpose interface card was constructed for the host computer. This interface card is a microprocessor-controlled device used for both program and buffer storage. This interface card buffers communication to and from the data acquisition system and identifies transmission errors.

V. REPEATABILITY AND ACCURACY DETERMINATION

To determine the repeatability and absolute accuracy of this test set, numerous tests were performed. These tests are described below.

To assure that the test set data reduction programs were capable of determining the conductivity in the presence of varying input signals, the following tests were made. The frequency markers were adjusted to be spaced at approximately 2-MHz intervals. Data were then acquired and stored on disk files for later investigation. These stored data were then operated on by the data reduction programs and the resultant conductivity inferred. The data reduction programs were then modified to use every other marker when linearizing the frequency axis. This simulated markers every 4 MHz. The conductivity was then inferred by the data reduction programs using every other marker. A similar procedure was done using every third marker, and thus it appeared to the data reduction program that the markers were spaced every 6 MHz. The results of these tests indicated that the conductivity estimation procedure was relatively insensitive to the exact number of markers used to compute the frequency axis. Also, based on the resonance width variations, an overall test set accuracy of approximately 1 percent plus cavity assembly/disassembly variations can be inferred.

To verify that the incident power levels at the detector D1 were

unimportant, measurements were made in which the cavity under test was unchanged and the input power was adjusted over a 10-dB range. The data reduction programs showed no discernible difference in the inferred conductivity over this range of input power. In the normal test procedure, the power at the detector D1 was kept nominally constant.

In any cavity measurement in which the cavity must be repeatedly assembled and disassembled, it is important to assure that this has no influence on the measurement. By virtue of the TE_{01} and TE_{02} measurement modes, the dependency on the cavity geometry is minimized. To assure that the assembly could be done repeatably, the cavity was assembled and disassembled numerous times, and the inferred conductivity was computed for each case. In each measurement, the torque used on the bolts which load the cavity was kept constant at 0.9 newton-meters (8 inches-pounds). In each case, the cavity was assembled in an identical manner. These results indicated that there was little dependence on the assembly procedure.

To verify that the measurement results were independent of the torque used to assemble the cavity, measurements were made at various torque levels. In each case, the cavity was assembled and torqued to 9 newton-meters (80 inches-pounds), and then the torque was lowered to the test value. This assured good mechanical contact. These tests indicated a slight dependency on torque when the torque levels measure zero. Therefore, in all tests small loads were placed on the cavity to assure good mechanical contact.

To verify that the test set results were independent in all respects of the iris coupling, tests were made on two sample sets that were identical except for the size of their irises. The diameters of the irises were 4.76 mm (0.188 inch) and 3.57 mm (0.141 inch). The sample set with the 4.76-mm diameter had an average measured conductivity of 4.559×10^7 S/m and the sample set with the 3.57-mm diameter had an average measured conductivity of 4.596×10^7 S/m. The TE_{02} mode was selected to excite both cavities. Their results gave confidence to the iris coupling model used.

Another experiment was performed to determine the effect of different excitation modes on the measured conductivity. Measurements made on a single sample set excited by the TE_{02} mode gave an average measured conductivity of 4.559×10^7 S/m. The sample set excited by the TE_{01} mode gave an average measured conductivity of 4.465×10^7 S/m. The closeness of these results indicate that the conductivity measurements are independent of the excitation mode.

VI. PLATING OF THE SAMPLES

Four sets of steel substrates, S1, S2, S3, and S4, were mechanically prepared for the conductivity measurement. Two cyanide copper-

plating baths (B1 and B2) were also prepared in accordance with the prescribed waveguide plating formula used at the Western Electric Forsgate Laboratory to prepare waveguide for the Bell Laboratories FET.[10] Both the time and current density parameters were adjusted to produce a 5-μm thick copper layer on each steel substrate. The copper cyanide baths used are identified as B1 and B2; they differ only in respect to their sodium cyanide (NaCN) and copper cyanide (CuCN) concentrations. The B2 modified copper cyanide bath is basically the same B2 bath mentioned above; however, due to some chemical depletion after plating, the B2 bath had to be regenerated, and thus the copper cyanide and sodium cyanide were replenished to readjust the basic B2 bath. Each set of substrates were processed and measured in the following manner. Set S1 was copperplated in the B1 copper cyanide plating bath, set S2 was copperplated in the B2 bath, and sets S3 and S4 were plated in the B2 modified bath.

VII. COPPER CONDUCTIVITY MEASUREMENT OF SAMPLE SETS S1, S2, S3, S4

In this part of the measurement, the average measured conductivity of the electrodeposited copper for sample set series S1, S2, S3, and S4 was found to be 4.278, 4.443, 4.837, and 4.873 $\times$ 10^7 S/m, respectively. These results are summarized in Table II. The measured variations in copper conductivity are due to bath composition and suggest that the electrical conductivity of electrodeposited copper can be extremely sensitive to the chemical composition of the plating bath.

VIII. CHROMATE TREATMENT AND MEASUREMENT OF TREATED SURFACES

In this next series of measurements, sample sets S2, S3, and S4 were treated with electrolytic chromate[10] and remeasured. The measured copper conductivity of these samples was found to be 4.381, 4.869, and 4.859 $\times$ 10^7 S/m, respectively. The results indicate that the chromate treatment caused little or no degradation of the copper surface.

Table II—Average copper conductivity measured

Sample Set ID	Copper Cyanide Plating Bath ID	Conductivity (σ) of Copper Plate	Copper Cyanide and Sodium Cyanide Concentrations	
			Sodium cyanide (NaCN)	Copper cyanide (CuCN)
S1	B1	4.278 $\times$ 10^7 S/m	10 oz./gal	9 oz./gal
S2	B2	4.443 $\times$ 10^7 S/m	13 oz./gal	8 oz./gal
S3	B2 modified	4.837 $\times$ 10^7 S/m	Added 10% to regenerate bath	Added 20% to regenerate bath
S4	B2 modified	4.873 $\times$ 10^7 S/m		

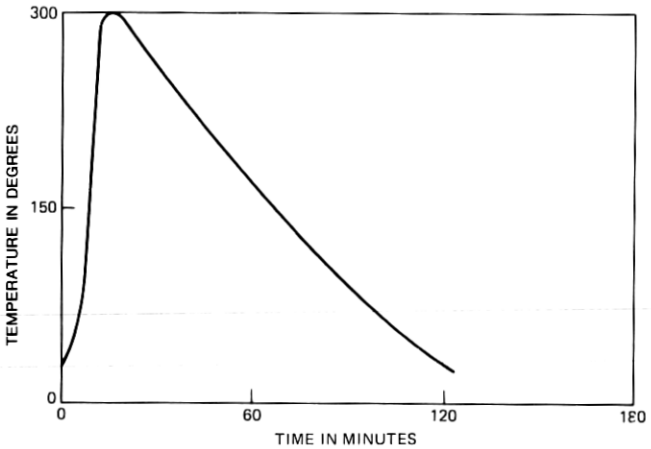

Fig. 7—Dielectric bonding temperature profile.

IX. SURFACE PREPARATION, BONDING, AND ANNEALING COPPER PLATE SAMPLES

Prior to the high temperature (300°C) polyethylene bonding process, sample set S2 was placed in a special bonding fixture, where a low-temperature (190°C) tacking technique prepared the polyethylene disks, in a vacuum, for the actual high-temperature bond. The disks were exactly the same diameter as the cavity and were 180-μm thick. Once the light tack has been accomplished, the samples are ready for the final bond.

Under program control, the high-temperature oven is purged with nitrogen for 30 minutes and, under positive nitrogen pressure, oven temperature increases linearly from room temperature to 300°C in 45 minutes, remaining at 300°C for 15 minutes, decreasing linearly to 50°C after 40 minutes. The temperature profile is shown in Fig. 7.

This step takes advantage of surface tension phenomena, preventing the polyethylene from running out of the controlled area as it becomes a fluid at 300°C.

X. MEASUREMENT OF BONDED/CHROMATE COPPERPLATED SURFACES

Upon completion of the heat treatment, sample set S2 was measured on the Q set, and the average copper conductivity of this set was found to be 4.776×10^7 S/m. A comparison of the measured conductivity before and after bonding indicates that the bonding process caused an increase in copper conductivity of approximately 8 percent. Since the S2 set was made in the same way as the WT4 FET waveguide product as far as laboratory conditions permitted, the increase in electrical conductivity after bonding suggests that the mechanism that caused

the unexpectedly low copper losses (5.16×10^7 S/m) measured in the FET occurred during the bonding of the polyethylene to the waveguide wall.

To further investigate the mechanism, the S4 sample set was chosen to simply repeat the previous S2 set experiment discussed above. The only difference between the S2 and S4 sample sets was the initial copper conductivity value of the plated copper end plates, which appears to be a direct result of the plating bath chemical concentration.

The remaining sample sets (S3 and S1) were used to isolate the exact mechanism that caused the increase in copper conductivity of sample set S2. Hence, S1 (untreated copper surface) and S3 (copper surface treated with chromate only) were scheduled to go into the high-temperature oven with S4. The goals of this experiment are summarized as follows: (*i*) using the S1 sample set, determine if only the annealing effects at 300°C cause the increase in electrical conductivity observed, and (*ii*) using the S3 sample set, determine if the increase in copper conductivity is a combination of chromate treating and annealing.

The three sets were placed in the high-temperature oven and exposed to the same nitrogen purge/fill and heat cycle described above for the S2 sample set. Next, each set was removed from the oven and measured on the Q set. The average measured copper conductivity of sample sets, S4, S3, and S1 was found to be 5.201, 5.399, and 4.802×10^7 S/m, respectively. It can be seen from the results that, in all three cases, copper only, copper/chromate, and copper/chromate/polyethylene, the copper conductivity increased. Thus, it was concluded that the common denominator isolated and identified as causing the increase in copper conductivity is the annealing effect at 300°C. These data are completely summarized in Table III. Also, it can be seen from the table that a larger increase, between 11 and 12 percent, occurred with the sample sets processed without the polyethylene. The polyethylene samples had an increase in copper conductivity between 7 and 8 percent.

XI. CONCLUSION

A test set capable of making precise copper conductivity measurements at millimeter-wave frequencies was developed.

Table III—Average copper conductivity ($\times 10^7$ S/m) vs treatment

	Sample set identification			
	S3	S4	S2	S1
1-Copper plate	$\sigma = 4.837$	$\sigma = 4.873$	$\sigma = 4.443$	$\sigma = 4.278$
2-Chromate	$\sigma = 4.869$	$\sigma = 4.859$	$\sigma = 4.381$	
3-Anneal at 300°C	$\sigma = 5.399$			4.802
4-Anneal and bond		$\sigma = 5.201$	$\sigma = 4.776$	

The overall accuracy of the test set was determined by examining the scatter in the data due to mechanical variations. Thus, for copper conductivities between 4.3 and 5.4 $\times$ 10^7 S/m, the test set accuracy was 3 percent. Repeated measurements made without dismantling the cavity gave accuracies about 1 percent. Hence, the overall experimental accuracy is to a large degree governed by assembly and disassembly of the cavity, and any improvements in the experimental accuracy will require improvements in the design of the cavity and fixture assembly.

Our measurements have shown that chromate surface treatments or the presence of polyethylene on electrodeposited copper surfaces have negligible effects on conductivity. However, annealing at 300°C in a nitrogen-filled oven was significant. Increases in conductivity as high as 12 percent were realized (4.837 to 5.399 $\times$ 10^7 S/m) for the S3 sample set case. The 5.399 figure represents a conductivity of 93 percent of the IACS value. The results are consistent with the reported results (89 percent IACS) taken during the WT4 field evaluation trial and reproduce in the laboratory the unexpected low loss measured. The bonding process in addition to bonding also provided for annealing of the copper plate, changing the copper crystal structure in such a manner as to enhance the electrical conductivity of the plate.

It has also been found that, to realize high conductivity in electrodeposited copper, careful attention must be given to the chemical compositions of cyanide copper plating baths. For example, in this experiment different baths, although basically identical, yielded different electrical conductivity values. Sample set S3 plated in bath B2 had a measured conductivity approximately 13 percent higher than sample set S1 plated in bath B1.

The laboratory test set results agreed with measurements on the 14-km waveguide run in the WT4 FET. The test set, therefore, is a suitable tool to evaluate various plating processes used at millimeter-wave frequencies in general and those used in waveguide manufacturing facilities in particular.

XII. ACKNOWLEDGMENT

The design of the test set and results reported here involved the efforts of others. In particular, the need for a highly accurate Q set was first suggested by R. D. Tuminaro, who also laid down some fundamental groundwork. W. C. Cohen of Western Electric participated in the design and implementation of the mechanical and plating fixtures. P. C. Milner and T. A. Palumbo of Department 1534 gave invaluable advice on plating.

In addition, the authors would like to thank D. A. Alsberg for his direction and support. The continuing support of W. D. Warters, J. M. Sipress, and D. M. Brady is also gratefully acknowledged.

APPENDIX A

Q-Set Measurement Theory and Derivations

A general expression for the unloaded Q, Q_0, of the TE$_{01}$ mode in a cylindrical cavity[11] is

$$Q_0 = \frac{\lambda_0[P_{01}^2 + (l\pi R/L)^2]^{3/2}}{2\pi\delta[P_{01}^2 + (2R/L)(l\pi R/L)^2]}, \tag{5}$$

where

δ = skin depth
P_{01} = first root of the derivative of the zero-order Bessel function
R = radius of cavity
L = length of cavity
$\lambda_0 = c/f$, c = speed of light, f = frequency
l = length of cavity in half wavelengths.

Similar expressions for the unloaded Q due to the individual losses in the cavity end walls and side walls can be derived:

$$Q_{0S} = Q_{\text{side wall}} = \frac{\lambda_0}{2\pi\delta_{\text{side}}} \frac{[P_{01}^2 + (l\pi R/L)^2]^{3/2}}{P_{01}^2}, \tag{6}$$

$$Q_{0E} = Q_{\text{ends}} = \frac{\lambda_0}{2\pi\delta_{\text{ends}}} \frac{[P_{01}^2 + (l\pi R/L)^2]^{3/2}}{(2R/L)(l\pi R/L)^2}. \tag{7}$$

The total loss of the cavity is the sum of the end- and side-wall losses. Since the losses are proportional to $1/Q$,

$$\frac{1}{Q_0} = \frac{1}{Q_{0E}} + \frac{1}{Q_{0S}}. \tag{8}$$

It can be shown that, in our case, the loss due to the side walls is negligible when compared to the loss due to the ends, as shown in Appendix B.

Neglecting the side-wall term* in eq. (8),

$$Q_{0E} = Q_0. \tag{9}$$

Solving for the skin depth of the ends, we get

$$\delta_{\text{ends}} = \frac{[P_{01}^2 + (l\pi R/L)^2]^{3/2}}{(2R/L)(l\pi R/L)^2} \left[\frac{\lambda_o}{2\pi Q_0}\right]. \tag{10}$$

Hence, if Q_0 is measured δ_{ends} is determined since the other parameters are known.

The skin depth is related to the conductivity (σ)[8] as follows:

---

* Actual data reduction algorithms did not neglect the side-wall term, but assumed a wall with conductivity 80 percent of the IACS value.

$$\sigma = \frac{1}{\pi f \mu_0 \delta_{\text{ends}}^2}, \tag{11}$$

where

f = frequency
μ_0 = permeability of vacuum ($4\pi \times 10^{-7}$ Henries/meter).

The problem of finding the conductivity is then one of accurately determining Q_0.

The loaded Q, Q_L is defined by

$$Q_L = \frac{f_0}{\Delta f}, \tag{12}$$

where f_0 is the center frequency of the resonance and Δf is the full width at half maximum power. Q_L is equal to the sum of all the losses (iris loss, side-wall loss, and end-wall loss). Thus, the total loss for a transmission cavity is:

$$L_T = L_{\text{iris1}} + L_{\text{iris2}} + L_{\text{walls}} \tag{13}$$

or assuming identical irises yields

$$L_T = 2L_I + L_W \tag{14}$$

and, since

$$\frac{1}{Q} \alpha \text{ loss}, \tag{15}$$

one arrives at the usual equation of loaded Q.

$$\frac{1}{Q_L} = \frac{1}{Q_0} + \frac{2}{Q_I}, \tag{16}$$

where $1/Q_I$ represents the loss of each iris. But[12]

$$\frac{Q_0}{Q_I} = \beta. \tag{17}$$

Substituting eq. (17) into eq. (16) yields an expression for Q_0,

$$Q_0 = Q_L(1 + 2\beta). \tag{18}$$

Our experiment measures Q_L, the loaded Q, and T, the transmission loss. The transmission loss T is related to β[12] by

$$T = \frac{P_L \text{ (power transmitted on resonance)}}{P_0 \text{ (power transmitted with cavity out of circuit)}}$$

$$= \frac{4\beta^2}{(1 + 2\beta)^2} \tag{19}$$

Solving for β, we get

$$\beta = \frac{\sqrt{T} + T}{2(1 - T)}. \tag{20}$$

Substituting eq. (20) into eq. (18), we get

$$Q_0 = Q_L\left(\frac{1}{1 - \sqrt{T}}\right). \tag{21}$$

For this study, the T measured is between 0.01 and 0.001 (large and small iris holes).

Hence, once the loaded $Q(Q_L)$ and the transmission loss (T) are measured, the metallic conductivity (σ) can be computed using eqs. (21), (10), and (11) above.

APPENDIX B

Cavity Side-Wall and End-Wall Losses

It can be shown that, in our case, the loss due to the side walls is negligible when compared to the loss due to the ends. Consider the ratio

$$\frac{\text{Loss}_{\text{side wall}}}{\text{Loss}_{\text{ends}}} = \frac{Q_{0E}}{Q_{0S}}. \tag{22}$$

Inserting the results of eqs. (6) and (7) of Appendix A in the above equation, we get the ratio

$$\frac{Q_{0E}}{Q_{0S}} = \frac{\delta_{\text{side}}}{\delta_{\text{ends}}} \frac{P_{01}^2}{[2R/L][l\pi R/L]^2}. \tag{23}$$

The equation can be simplified as follows:

$$P_{01} = \frac{2\pi R}{\lambda_c} \qquad \text{(Ref. 8)}, \tag{24}$$

where λ_c = cutoff wavelength for the TE_{01} mode. For a half wavelength long cavity

$$\frac{L}{l} = \frac{\lambda_g}{2}, \tag{25}$$

where λ_g = guide wavelength.

Also note that λ_g is related to λ_c and λ_o by the relationship

$$\frac{1}{\lambda_g^2} = \frac{1}{\lambda_o^2} - \frac{1}{\lambda_c^2}. \tag{26}$$

Substituting the above relations into (6), we get the ratio

$$\frac{\text{Loss}_{\text{side wall}}}{\text{Loss}_{\text{ends}}} = \frac{\delta_{\text{side}}}{\delta_{\text{ends}}}\left[\frac{L}{2R}\left[\frac{1}{(\lambda_c/\lambda_o)^2 - 1}\right]\right]. \tag{27}$$

For our case, the values of the parameters are

$$L = 0.00381 \text{ meters}$$
$$R = 0.020 \text{ meters}$$
$$\lambda_c = 1.64R$$
$$\lambda_o = 0.00714 \text{ meters (at 42.6 GHz)}.$$

Thus

$$\text{Ratio losses} = 0.0047\,\frac{\delta_{\text{side}}}{\delta_{\text{ends}}}. \tag{28}$$

The ratio, $(L/2R)[1/[(\lambda_c/\lambda_o)^2 - 1]]$, is shown for various cavity radii at 42 GHz in Fig. 8. Since both the side wall and ends are copperplated on steel, $\delta_{\text{side}} \approx \delta_{\text{end}}$, the loss due to the side walls is negligible compared to that of the ends.

APPENDIX C

Data Reduction

The raw data from the microprocessor data acquisition system is stored in the host processor on disk files. These files are then manip-

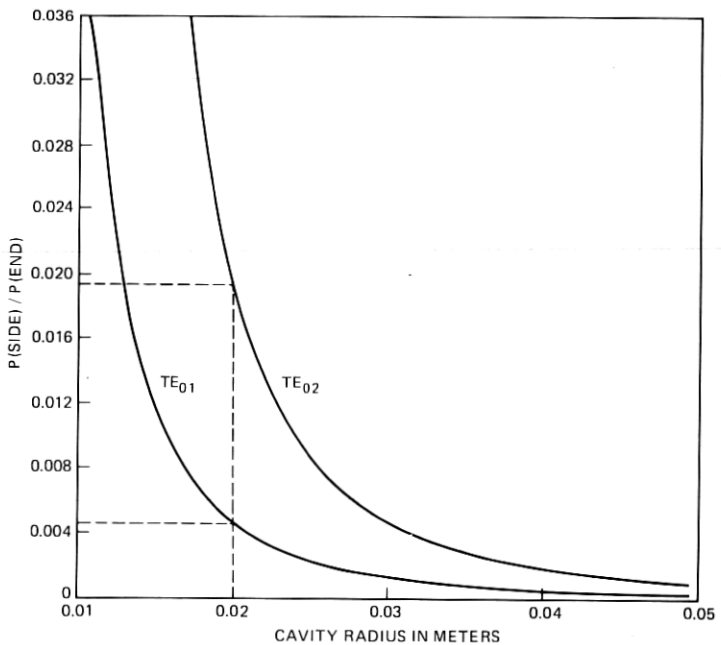

Fig. 8—Side loss vs radius at 42 GHz.

ulated by the various data reduction algorithms. Corrections are made for the nonlinear sweep and then theoretical resonance shapes are fit to the experimental data. Three separate measurements are made by the data acquisition system. In each measurement, two channels are digitized simultaneously. These are the power transmitted and the frequency markers.

The first measurement is the power transmitted through the cavity and is the standard resonance waveform, which is distorted by the nonlinear sweep of the klystron. The second measurement is with the cavity removed. This measurement represents the power versus frequency output of the klystron. This measurement is necessary because the klystron's power output is not constant over the full sweep range. The third measurement is with no cavity and no power transmitted to the detector. This measurement is used to form the base line for the detector. The third measurement is always subtracted from the first two measurements. The third measurement is not used for any other data reduction but contains any systematic or coherent noise that is not removed by the signal averaging process.

It is assumed that the output voltage of the diode detector D1 is proportional to the incident power. Thus the diode is operated in the square-law region. To insure this square-law operation, the input power is varied to the diode and the resultant voltage is observed. The bias on the diode is adjusted until square-law performance is obtained over the dynamic range of interest.

The cavity response is sampled every 55 ms. The operating frequency of the klystron must be accurately determined for each sampled point. The frequency sweep characteristic of a klystron is not linear with time, even though the sweep voltage is linear, and thus an accurate estimate of the frequency at each sample time is required. This conversion from time to frequency is done with the aid of the marker data. The peaks of the markers are at equal intervals of frequency. The host computer generates a table of marker peak position (in time) versus marker frequency. The frequency for each sampled point is then interpolated by using this look-up table. The interpolation technique used is the least-squares cubic spline.[13]

The model for the amplitude of the transmitted rf signal is

$$A = \frac{A_0}{1 + (f - f_0/\Delta f)i} + (D + iE). \tag{29}$$

The first term represents the standard resonance structure with center frequency f_0 and a full width at half maximum of Δf. The term f is the frequency of the transmitted signal, and A_0 is the amplitude of the signal on resonance.

The second term represents a leakage term and was included in the

model because of the proximity of the two iris holes. It should be expected that the contribution of the leakage term should be small. This term represents the amplitude of the rf that would be transmitted through the cavity structure far from resonance.

The square-law diode detector used in this experiment measures only transmitted power and thus, from eq. (30), the transmitted power model is

$$P_t = |A|^2$$

$$P_t = \frac{R_1 - \gamma R_5}{1 + \gamma^2} + R_4, \tag{30}$$

where

$$\gamma = (f - f_0/\Delta f)$$

$$R_1 = A_0^2 + 2A_0 D$$

$$R_4 = D^2 + E^2$$

$$R_5 = 2A_0 E.$$

Equation (30) represents the mathematical model used to represent the power transmitted through the cavity and measured by the test set. Fitting the data to eq. (30) requires the use of nonlinear least-squares techniques.[14]

Nonlinear least squares inherently require initial values for the model parameters. These parameter values are then iterated upon until they converge.

Because the leakage was small, the leakage term is set to zero as an initial estimate,

$$D = 0$$

$$E = 0.$$

The term R_1 was set to the peak transmitted power, and f_0 is set to the true frequency at which the peak was measured. The initial Δf was estimated by finding the width of the resonance at the two frequencies at which the power is half the measured peak power.

Thus, the initial estimates for the fitting algorithm are the very terms used by most investigators as the final result.

To aid the data reduction algorithm convergence, it is assumed that the leakage term is zero and the terms A_0, f_0, and Δf are estimated. When these terms are estimated more accurately, then the leakage term is allowed to become nonzero. The fitting scheme used typically requires two iterations to converge when the leakage term is confined to zero and two more iterations to estimate all five adjustable parameters.

It should be noted that extreme care must be exercised when estimating the parameters of eq. (30) because the matrices involved are inevitably nearly singular. To address this problem, singular value decomposition was used when simultaneous linear equations are to be solved.[13]

Because the line shape being estimated is nearly Lorentzian (i.e., it falls off as $1/f^2$ for large f), the tails can have a large effect on the values of the parameters being estimated. The residuals (the difference between the data and the model) provide an excellent mechanism for determining the degree of the fit. For the resonances measured, Δf was approximately one-tenth the frequency of the measured klystron sweep. The resonances measured and fit with the model of eq. (30) had typical standard deviations of:

$$\mathrm{SD}_{\mathrm{typical}} = 0.010 * \text{resonance peak power.}$$

The standard deviation of the model using the initial guess parameters was typically 50 percent higher than the final standard deviation after the nonlinear least-squares algorithm had converged.

To determine the effect of the tails on the estimated parameters, another strategy was used. Weighted nonlinear least squares were used to determine the effect of the tails. This technique allows the fitting algorithm to fit various data less accurately. In other words, certain parts of the data are considered more important than others. If a data point is considered important, then the fitting routine is required to adjust the model parameters to force the model to be close to those data points. The weighting factor used is:

$$W = \left[\frac{1}{1+\gamma^2}\right]^n, \tag{31}$$

where n is some value between 0 and 2. This expression is a Lorentzian line shape raised to a power. It is just the line shape that would be estimated if no rf leakage was involved.

In the actual data reduction, five least-squares fits were used; the data in each case were weighted differently. The various weights determined the relative importance of the data points. The five weights used had values of 0, 0.5, 1.0, 1.5, and 2. The zero weight corresponds to equal weighting of all points; the 0.5 to 2 weights increase the importance of the higher data values (data close to resonance). From these least-squares fits, the Qs and corresponding conductivities were computed.

If the resonance is not contaminated, the estimates of Δf should be the same for any value of n. This criterion provided a measure of the uncertainty of the results.

REFERENCES

1. J. C. Anderson, J. W. Carlin, D. J. Thomson, and T. J. West, "Field Evaluation Test-Transmission Medium Achievements," B.S.T.J., *56*, No. 10 (December 1977), pp. 2157–2178.
2. J. W. Carlin and P. D'Agostino, "Normal Modes in Over-Moded Dielectric Lined Circular Waveguide," B.S.T.J., *52*, No. 4 (April 1973), pp. 453–486.
3. T. S. Thorpe, "RF Conductivity in Copper at 8 mm Wavelengths," Proc. Inst. Elec. Eng., *101*, Pt. III (1954), pp. 357–359.
4. A. D. Merriman, *A Concise Encyclopedia of Metallurgy*, New York: Elsevier, 1965, pp. 407.
5. F. J. Tischer, "Surface Resistance of Single-Crystal Copper in the mm-Wave Region at Room Temperature," Surface Science, *44* (1974), pp. 411–420.
6. F. J. Tischer, "Excess Conduction Losses at Millimeter Wavelengths," IEEE Trans. Microwave Theory and Techniques, *MTT-24*, No. 11 (1976), pp. 853–858.
7. S. Hatano and F. Nihei, "Measurement of Surface Resistance in Oversized Circular Waveguide at Millimeter Wavelengths," IEEE Trans. Microwave Theory and Techniques, *MTT-24*, No. 1 (1976), pp. 886–887.
8. S. Ramo, J. R. Whinnery, and T. Vanduzer, *Fields and Waves in Communication Electronics*, New York: John Wiley, 1965, pp. 429–434.
9. M. A. Gerdine, "A New TE10-TE01 Mode Transducer for MM-Waves," Microwave J., *13*, No. 2 (1970), pp. 73–75.
10. R. J. Boyd, Jr., W. E. Cohen, W. P. Doran, and R. D. Tuminaro, "Waveguide Design and Fabrication," B.S.T.J., *56*, No. 10 (December, 1977), pp. 1873–1897.
11. R. E. Collin, *Foundations for Microwave Engineering*, New York; McGraw-Hill, 1966, p. 326.
12. E. L. Ginzton, *Microwave Measurements*, New York: McGraw-Hill, 1957, pp. 403–404.
13. C. L. Lawson and R. J. Hanson, *Solving Least Square Problems*, Englewood Cliffs: Prentice-Hall, 1974.
14. J. T. Betts, "Solving the Nonlinear Least Square Problem: Application of a General Method," J. Optimization Theory Appl., *18*, No. 4 (April 1976).